Crashworthiness assessment of auxetic foam-filled tube under quasi-static axial loading

Article *in* Materials and Design · September 2015

DOI: 10.1016/j.matdes.2015.08.152

CITATIONS
54

READS
1,002

5 authors, including:

Saeid Mohsenizadeh
Universiti Teknologi Malaysia
6 PUBLICATIONS **89** CITATIONS
SEE PROFILE

Roozbeh Alipour
Islamic Azad University, Mahshahr Branch
22 PUBLICATIONS **169** CITATIONS
SEE PROFILE

Mozafar Shokri Rad
Lorestan University
7 PUBLICATIONS **132** CITATIONS
SEE PROFILE

Ali Farokhi Nejad
Universiti Teknologi Malaysia
35 PUBLICATIONS **153** CITATIONS
SEE PROFILE

Materials and Design 88 (2015) 258–268

Contents lists available at ScienceDirect

Materials and Design

journal homepage: www.elsevier.com/locate/jmad

Crashworthiness assessment of auxetic foam-filled tube under quasi-static axial loading

S. Mohsenizadeh [a], R. Alipour [b,*], M. Shokri Rad [a], A. Farokhi Nejad [a], Z. Ahmad [a]

[a] Department of Applied Mechanics and Design, Faculty of Mechanical Engineering, Universiti Teknologi Malaysia, 81300, Johor Bahru, Malaysia
[b] Department of Mechanical Engineering, Mahshahr Branch, Islamic Azad University, Mahshahr, Iran

ARTICLE INFO

Article history:
Received 10 May 2015
Received in revised form 25 August 2015
Accepted 31 August 2015
Available online 4 September 2015

Keywords:
Auxetic foam
Energy absorption
Thin-walled tube
Crashworthiness
Negative Poisson's ratio

ABSTRACT

This present study investigates experimentally and numerically the crush response and energy absorption performances of auxetic foam-filled square tubes under quasi-static axial loading. Three different structures: empty, conventional and auxetic foam-filled square tubes have been compared and examined with respect to the deformation modes and load–displacement curves. Standard compression tests were conducted on the tubes to evaluate the influence of auxetic foam in the energy absorption of empty tubes. Moreover, results from computer simulation have also been supplemented to further examine the abovementioned effect. It is discovered that the auxetic foam-filled square tube is superior to empty and conventional foam-filled square tubes in terms of all studied crashworthiness indicators.

1. Introduction

Thin-walled structures are broadly designed and used in crashworthiness applications such as automotive, aeronautical and collision safety protection structures to absorb and dissipate the direct impact forces [1]. When subjected to a collision, thin-walled structure absorbs kinetic energy through plastic deformation due to progressive crushing. The metallic thin-walled tube is a widespread energy absorbing device owing to impressive folding deformation when subjected to axial compression. Moreover, thin-walled tubes have generally low cost, low weight, high ductility and ease of production [2–4]. Therefore, these structures have received extensive attention. Over the past decades, numerous studies have been carried out to improve the energy absorption and energy dissipation of metallic thin-walled tubes via changing the material characteristics, geometry, wall thickness and locating material filler inside them [5–13].

One of the most important goals in designing and energy absorbing device is to absorb maximum energy with minimum mass. To obtain a lightweight design, cellular materials such as foams have great energy absorption performance as they can endure large deformation at almost constant load [14]. As the importance of understanding the crushing behavior of foam-filled tubes (FFT) is increasing, several studies have been conducted using theoretical, numerical and experimental methods in recent years. Gupta and Ray [15] studied the collapse of 'as-received' and 'annealed' thin-walled empty and filled square tubes under lateral loading theoretically and experimentally. The filler material was in the form of polyurethane foam or Kail wood. Experimental and numerical study on circular aluminum alloy 6060-T4 filled with hydro aluminum AS foam under axial and oblique quasi-static loading was conducted by Børvik et al. [16]. Results concluded that the influence of foam filler is more pronounced for the mean crushing load than for the peak load. In other aspect, Santosa et al. [17] realized that the increase of the mean crushing load of a filled tube has a linear dependence with the foam compressive resistance and cross-sectional area of the tube. In addition, Aktay et al. [18] investigated the quasi-static axial crushing of extruded polystyrene aluminum FFT. In this study a numerical investigation of the crushing issue has been validated by a series of experiments to specify proportional models for filled tubes. Gameiro and Cirne [19] studied circular dynamic axial crushing of aluminum tubes of different geometries, empty and filled with micro-agglomerate cork. Results indicated that the ratio of tube diameter to the thickness and length of tube known as slenderness are significant parameters that globally govern the percentage increase in energy absorbed by tubular structures after cork-filling during impact loading. In numerical parametric studies, Ahmad and Thambiratnam [20–22] found that using foam-filler materials in conical thin-walled tubes assist in improving the crushing stability and collapse mode of a structure, resulting in great crashworthiness performance in both axial and oblique forces in the mode of quasi-static and impact loading. In a similar study, Mirfendereski et al. [23] carried out a parametric study to quantify the quasi-static and dynamic crush load and energy absorption response of empty and foam-filled tapered rectangular tubes to simplify their applications as energy absorbers. Number of oblique sides in loading, foam

* Corresponding author.
E-mail address: aroozbeh2@live.utm.my (R. Alipour).

http://dx.doi.org/10.1016/j.matdes.2015.08.152
0264-1275/

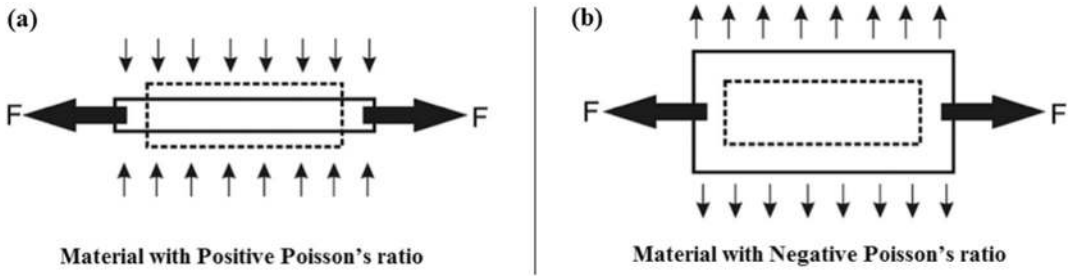

Fig. 1. Schematic behavior of material with (a) PPR and (b) NPR [48].

density and boundary conditions were parameters investigated in their research. The effect of low density filler material, such as aluminum honeycomb or foam, on the axial crash behavior of square box tube subjected to quasi-static loading was evaluated by Santosa and Wierzbicki [24].Recently, the potential utilization of integral-skin foams as stiffening elements located in thin-walled tubes known as ex situ FFT has been reported by Duarte et al. [25,26]. Also, some research has been focused on using functionally graded foam as the filler in thin-walled tubes aimed to improve crashworthiness efficiency [27,28]. Investigation in the mentioned literature shows that energy absorbing efficiency of thin-walled tubes may be improved by using foam fillers. However, FFTs are not necessarily preferable to non-filled tubes [14]. Aside from geometrical specification of tubes, the filler material can significantly influence some crashworthiness indicators such as specific energy absorption (SEA). This effect arises from several factors such as density and mechanical properties of fillers. Diversity of materials used as filler in the tube illustrates the mentioned fact.

All the materials inserted in the tubes mentioned in the literature have a level of capacity to absorb energy. One of the most common specifications is to have a positive Poisson's ratio (PPR). There is another generation of material which has negative Poisson's ratio (NPR). In contrast with PPR materials, materials possessing NPR have a counterintuitive behavior and exhibit an uncommon property of becoming contracted transversely when compressed longitudinally and vice versa [29,30]. This type of material has been named auxetic by Evans [31] and described in details by Love [32]. There are several references to describe, manufacture and investigate the behavior of auxetic materials such as foams [33–37]. The NPR feature of auxetic materials brings us a lot of remarkable capabilities such as better fracture toughness, increased strength, good acoustic behavior, superior energy dissipation and absorption and improved damping and indentation resistance [38–41]. The applications of these structures in some industrial cases have continuously been evaluated [42–47].

Although several studies have contributed to auxetic foams in the area of manufacturing, mechanical behavior and various applications, the authors could not find a direct discussion focused on using auxetic foams as filler inside thin-walled tubes. The aim of the present study is to assess the effects of using auxetic foam inside thin-walled tubes for enhancing the crashworthiness performance in comparison with conventional foam-filled and empty tubes. This study also highlights the possibility of using finite element techniques in simulation of auxetic material behavior in impact and crashworthiness applications.

2. Brief theory of auxetic foam

As mentioned in the Introduction section, conventional materials show PPR, so that their cross-section becomes smaller in tension and larger in compression, and vice versa for the NPR materials. A schematic of the behavior of both materials are shown in Fig. 1. The NPR class of material is known as “auxetic”, derived from the Greek word “auxetikos” which means “tendency to increase” [46].

Auxetic foams, generally produced by the open cell foam, are a treasured class of various auxetic materials due to their low price, easy availability and fabrication method. Methods to convert conventional foams into auxetic have been extensively researched. The concept of auxetic foams was proposed by Kolpakov [49]. Lakes [50] was the first to report

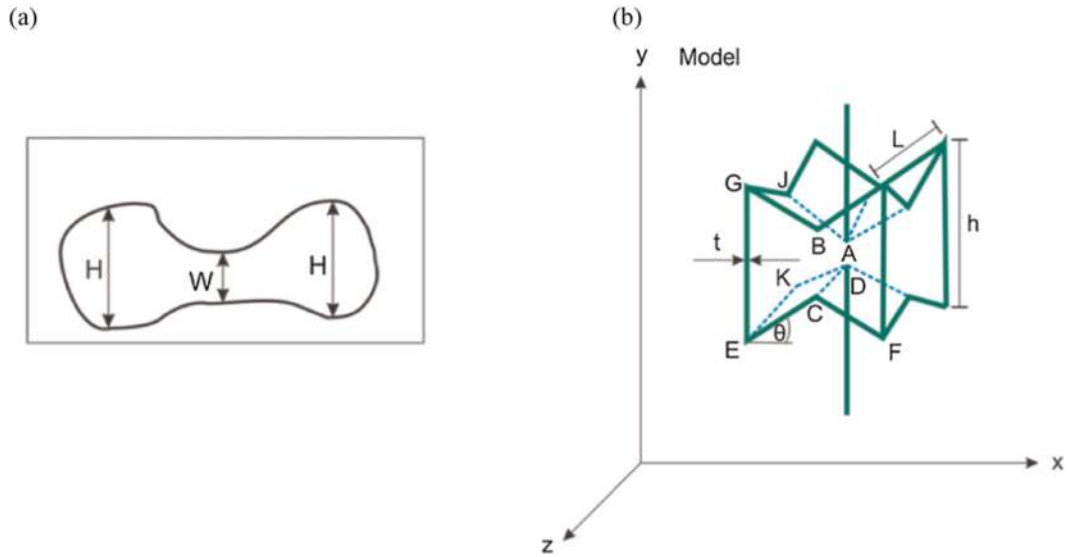

Fig. 2. Schematic of; (a) a 2D auxetic re-entrant foam cell, (b) a 3D model of an auxetic foam cell [59].

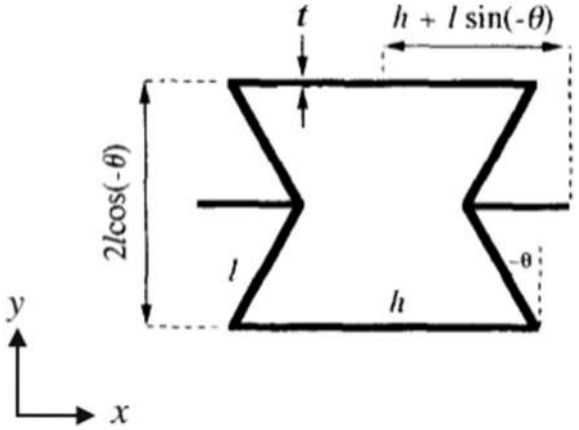

Fig. 3. Schematic of a 2D basic hexagonal unit cell for an auxetic structure [61].

a manufacturing process of auxetic foams via converting a metallic or polymeric conventional foam. Multi-phase auxetic fabrication was proposed by Bianchi et al. [33] who modified the fabrication process by combining a re-conversion back to conventional foam via a shape memory polymer operation followed by a second auxetic conversion. Friis et al. [51] suggested that the thermal transformation technique applied for thermoplastic foams could also be utilized on metallic foams, although this may be difficult because of the higher melting points of metals. Solvent-based auxetic fabrication [52], vac-bag auxetic fabrication [36] and dual density auxetic fabrication [53] are the other typical methods for converting conventional polymeric foams into the auxetic.

In the case of mechanical properties approach, reports [36,37,46,53] show that the conversion process of conventional foams into auxetic improves the mechanical properties. Many of these observations have been directly attributed to the enhancement of foam density due to the volumetric compression ratio applied and the change in the cellular structure [54–57]. The abovementioned variations lead to the changes in four elastic properties of the material: volumetric change under strain, stiffness, compressibility and rigidity which are respectively described by Poisson's ratio, Young's modulus, bulk modulus and shear modulus [48]. Choi and Lakes [58] discovered that the energy density of auxetic foam becomes greater compared to conventional types under large non-linear deformation.

There is an approach to calculate some mechanical properties of auxetic foams with respect to their microstructures. For instance, in one of the most comprehensive studies, Chan and Evans [59] modeled the cell geometries and volumes in 2D and 3D for auxetic foams. It was realized that the cell geometry becomes similar to the bow-tie re-entrant microstructure to some extent (Fig. 2) when the conventional foam is converted into auxetic foam.

After measuring the dimensions of the cells and averaging, the dimensions of the model were calculated based on the similarity of strain energy. From the strain energy point of view, the elastic modulus and Poisson's ratio for one of the faces of re-entrant structure (Fig. 3) shown in Fig. 2(b) can be expressed by Eqs. (1) and (2), respectively [60].

$$E_1 = k\frac{\left(\frac{h}{l}+\sin\theta\right)}{b\cos^3\theta} \tag{1}$$

$$\upsilon_{12} = \frac{\sin\theta\left(\frac{h}{l}+\sin\theta\right)}{\cos^2\theta} \tag{2}$$

where h, l and θ are as defined in Fig. 6 and b is the depth of unit cell. The value of k can be calculated using Eq. (3).

$$k = Eb\left(\frac{t}{l}\right)^3. \tag{3}$$

The term of E is the intrinsic Young's modulus and t is displayed on Fig. 3. Details of analytical solution and numerical result of the 3D re-entrant structure of auxetic material have previously been published in [34].

3. Fabrication and experimental procedure

Fabrication method and experimental procedure used are presented in this section. The energy absorption of three types of thin-walled square tubes; empty square tube (EST) conventional foam-filled square tube (CFFST) and auxetic foam-filled square tube (AFFST) subjected to quasi-static loading are experimentally studied.

3.1. Material preparation

3.1.1. Fabrication process of auxetic foams

The fabrication process of foam consists of two steps: fabricating the conventional polyurethane foam and converting the conventional foam into the auxetic.

In this research, conventional polyurethane foam was fabricated by mixing a suitable weight ratio of two chemical compounds which were Polyol and Isocyanate. According to other researches, the stiffness of the foam is too dependent on the weight ratios [62]. After mixing the compounds, the mixture was poured into a mold. The mold was then capped and kept at room temperature for more than two hours. The conventional polyurethane foam was ready in the three mentioned steps. Fig. 4 shows the different steps of the fabrication process.

Fig. 4. Different steps of polyurethane foam fabricating; (a) mixing, (b) pouring in the mold, (c) capping the mold.

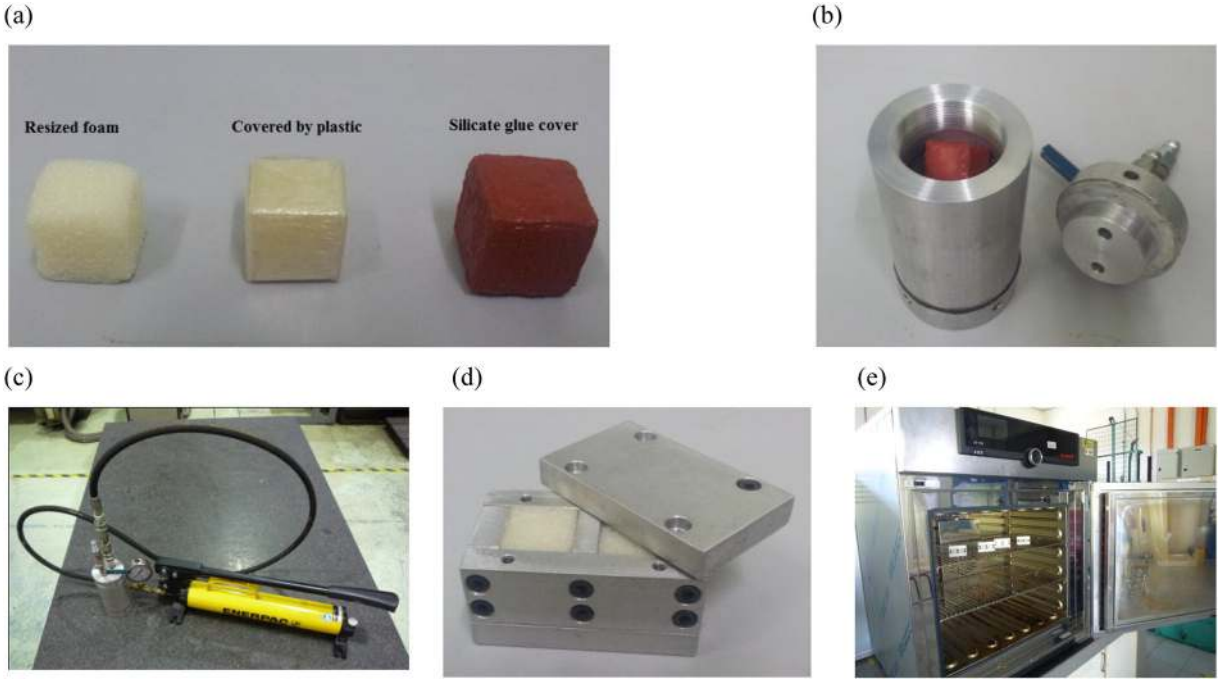

Fig. 5. Different steps of converting process; (a) cutting and covering, (b) cylindering and sinking, (c) applying pressure, (d) molding, (e) heating in the oven.

Next stage after fabricating the conventional foam was to convert it to the auxetic. This converting process consisted of the following steps. First the fabricated polyurethane foam was cut into favored cubic specimens using a foam cutter. These specimens were then put in a thick-walled aluminum cylinder (both closed-end) and immerse in hydraulic oil. To avoid oil penetration, the foam specimens were covered with the plastic cover and silicate glue. A hydraulic oil pump (able to apply pressure between 5 and 50 bar) was used to apply a hydro-static pressure on the specimens. After that, the specimens were placed in an aluminum mold and put inside an oven to be heated to 160 °C as the softening temperature. The final step of converting process was to cool down of specimens at the ambient temperature. The different steps of converting process and equipment used are shown in Fig. 5.

3.1.2. Material specification

The tube samples were simple square cross-section tubes made from 1 mm aluminum sheets for ease and affordability. The heights and cross-section of the tubes were 50 mm and 26 × 26 mm, respectively. The mechanical properties of the samples were determined based on ASTM E8M standards.

In order to determine the density of the foams, the specimens were measured and weighed prior to testing. Uniaxial compression tests of square cubes of foam according to ASTM D3574-95 were conducted to extract the stress–strain curve for both conventional and auxetic foams.

Although the Poisson's ratio of material can be normally calculated using strain gauging, this method is not precise, reliable or accurate enough for flexible material such as foam. In order to have better accuracy, specimens were initially subjected to a uniaxial compression test. During the test, a high-speed camera was used to capture the elastic deformation of foams at the different compression stages. Using image processing technique and based on observed deformation in the different directions, perpendicular strain and longitudinal strain were determined. Finally, Poisson's ratio was calculated by dividing the negative perpendicular strain with longitudinal strain [63]. Stress–strain curves of aluminum tube and foams are displayed in Fig. 6. The specifications of materials are listed in Table 1.

3.2. Experiments

The initial geometry of specimens is shown in Fig. 7. Each test includes 5 samples in which the average data was used for the

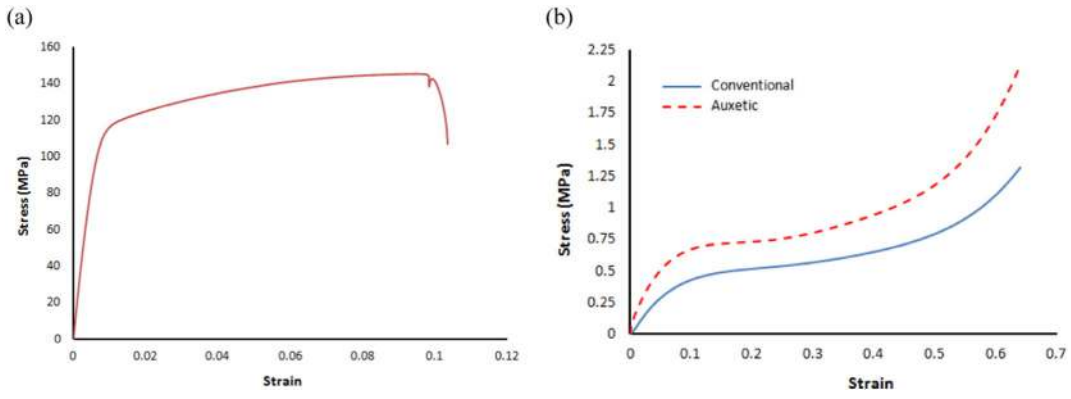

Fig. 6. Stress–strain curves of; (a) aluminum, (b) foams.

Table 1
Mechanical properties of aluminum tube and foams.

Property	Symbol	Value		
		Aluminum	Conventional foam	Auxetic foam
Young's modulus	E (GPa)	56	5.2	9.6
Initial yield stress	σ_y (MPa)	115	0.51	0.36
Poisson's ratio	υ	0.33	0.01	−0.26
Density	ρ (kg/m^3)	2700	58	96

crashworthiness assessment. Quasi-static compression test on the samples was done by using an INSTRON universal testing machine as shown in Fig. 8. The loading rate was set to 1.5 mm/min. The samples were compressed up a crush length of 30 mm.

4. Finite element analysis

In the present study, the computer simulations were conducted using the nonlinear finite element (FE) code ABAQUS/Explicit. Models of the square tubes were developed using hexahedral elements with 8 nodes which appropriately simulated the buckling mode of the tubes. Auxetic and conventional foam were modeled using 8 node solid elements with hourglass control. Stiffness-based hourglass control was employed to avoid zero energy deformation modes. After convergence, element sizes of 1 mm for the tubes and 1.9 mm for the foam filler were chosen to achieve acceptable results.

A rigid body was used for the jaws. Surface-to-surface contact was used for contact between the jaws and the tubes and also between tubes and foams. Self-contact was also used for the tube wall and foam itself. The friction coefficient between foam and tube were equaled to 0.19 [64]. The lower jaw was stationary and the upper one moved downward up to 30 mm crush length with a loading speed of 1.5 mm/min, similar to experiments. Identical boundary conditions to experimental set-up were applied to all models using a couple of reference points. Upper jaw was fixed in all degrees of freedom except for along loading direction. The lower jaw was fixed in all degrees of freedom. Explicit dynamic solver was used for simulation. A finite element model of a sample is shown in Fig. 9.

4.1. Simulation of tube behavior

The isotropic plasticity model was employed to simulate the tubes. The plastic hardening behavior of the tubes was calculated using Eqs. (4) and (5) and data obtained in Fig. 6(a).

$$\sigma_T = \sigma_E(1+\varepsilon_E) \tag{4}$$

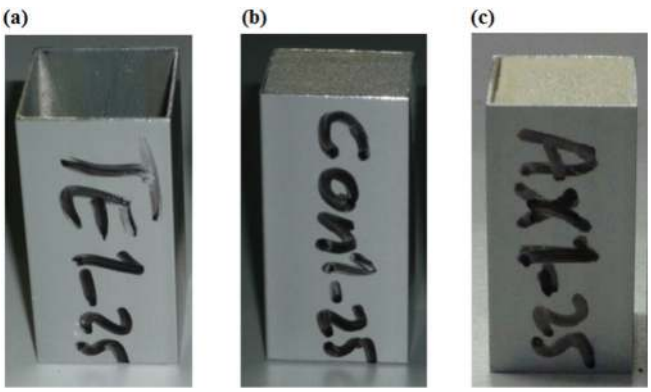

Fig. 7. Tube configuration; (a) EST, (b) CFFST, (c) AFFST.

Fig. 8. Loading process of a sample.

$$\varepsilon_T = \ln(1+\varepsilon_E) - \frac{\sigma_T}{E} \tag{5}$$

where σ_E and σ_T are the engineering and true stresses, respectively. In similar, ε_E and ε_T are the engineering and true plastic strains.

4.2. Simulation of foam behavior

Since the behavior of foam is different from that of metal, classical plastic theory cannot be used to describe their behaviors. Therefore, some constitutive models have been developed, so that the yield surface depends on both the mean stress and the Von Mises equivalent stress. Also all of them are phenomenological models [65].

In this study, the constitutive model is typically used in energy absorption structures based on the volumetric hardening during loading process. This model is devoted a yield surface with an elliptical dependence of deviatoric stress on pressure stress in the meridional plane [66].

The yield function (F) for crushable foam materials is defined in terms of the Kirchhoff stress and given by Eq. (6) [67].

$$F = \sqrt{q^2 + \alpha^2(p-p_0)^2} - B \tag{6}$$

where q is the Von Mises equivalent stress and p is the mean stress. The parameters p_0 and B of the yield ellipse are related to the yield

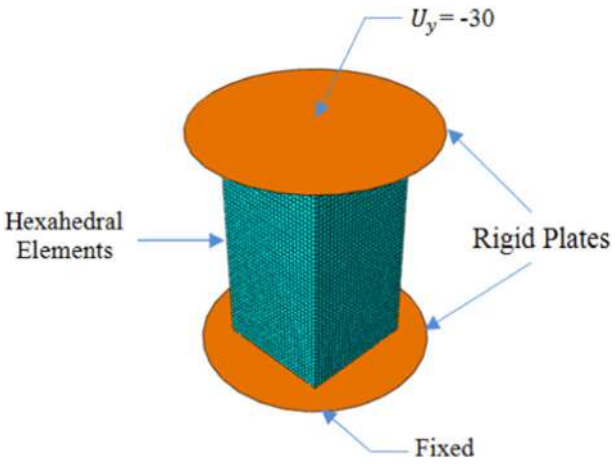

Fig. 9. A finite element model of samples.

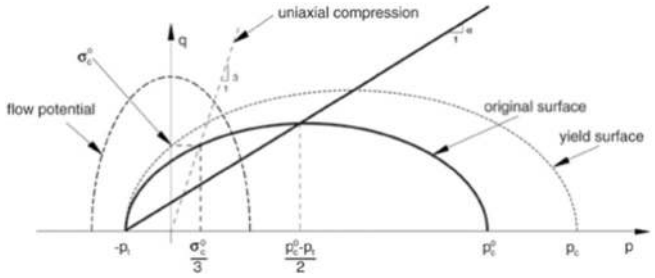

Fig. 10. Yield surfaces and flow potential for the volumetric hardening.

strength in hydrostatic compression (p_c) and to the yield strength in hydrostatic tension (p_t). Then, p_0 and B are calculated by Eqs. (7) and (8).

$$p_0 = \frac{p_c - p_t}{2} \tag{7}$$

$$B = \alpha\left[\frac{p_c + p_t}{2}\right]. \tag{8}$$

The parameter α represents the shape factor of the yield ellipse in the p–q stress plane and can be calculated as

$$\alpha = \frac{3k}{\sqrt{(3k_t + k)(3 - k)}} \tag{9}$$

$$k = \frac{\sigma_c^0}{p_c^0} \tag{10}$$

$$k_t = \frac{p_t}{p_c^0} \tag{11}$$

where σ_c^0 and p_c^0 are the initial yield strength in uniaxial compression and the initial yield strength in hydrostatic compression, respectively.

Eq. (6) represents an elliptical yield surface in the stress plane of Von Mises stress versus the mean stress as illustrated in Fig. 10 [67].

The plastic strain rate for the volumetric hardening model is as follows.

$$\varepsilon^{Pl} = \varepsilon^{pl}\frac{\partial G}{\partial \sigma} \tag{12}$$

where ε^{pl} is the equivalent plastic strain rate and G is the flow potential, (Eq. (13)).

$$G = \sqrt{q^2 + \beta^2 p^2}. \tag{13}$$

The parameter β represents the shape factor of the yield ellipse and the ellipse for the flow potential which is determined via Eq. (14).

$$\beta = \frac{3}{\sqrt{2}}\sqrt{\frac{1 - 2\nu_p}{1 + 2\nu_p}} \tag{14}$$

where ν_p is the plastic Poisson's ratio given by

$$\nu_p = \frac{3 - k^2}{6}. \tag{15}$$

The yield surface intersects the p-axis at $-p_t$ and p_c as shown in Fig. 10. It is assumed that p_t remains fixed throughout any plastic deformation process. By contrast, the compressive strength, p_c, evolves as a result of compaction (increase in density) or dilation (reduction in density) of the material. The evolution of the yield surface can be expressed through the evolution of the yield surface size on the hydrostatic stress axis as a function of the value of volumetric compacting plastic strain, $-\varepsilon_{vol}^{pl}$. With a constant p_t, this relation can be obtained from a user-provided uniaxial compression test data using Eq. (16) [68].

$$p_c\left(\varepsilon_{vol}^{pl}\right) = \frac{\sigma_c\left(\varepsilon_{axial}^{pl}\right)\left[\sigma_c\left(\varepsilon_{axial}^{p_t}\right)\left(\frac{1}{\alpha^2} + \frac{1}{9}\right) + \frac{p_t}{3}\right]}{p_t + \frac{\sigma_c\left(\varepsilon_{axial}^{pl}\right)}{3}} \tag{16}$$

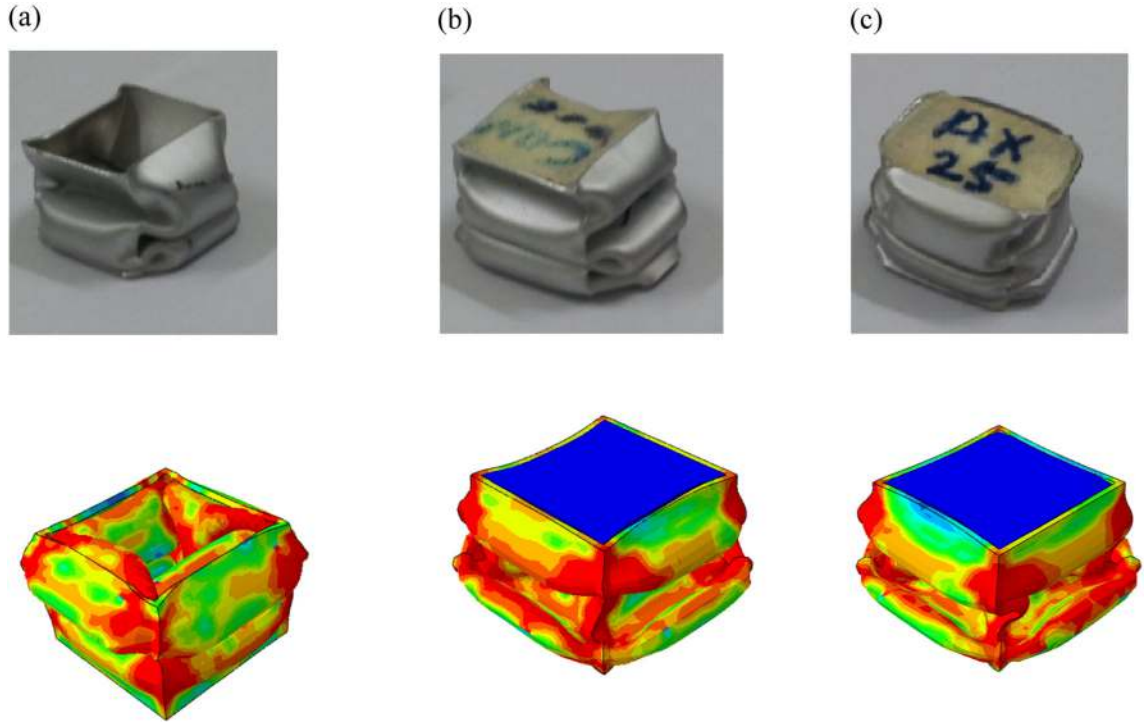

Fig. 11. Deformation modes; (a) EST, (b) CFFST, (c) AFFST.

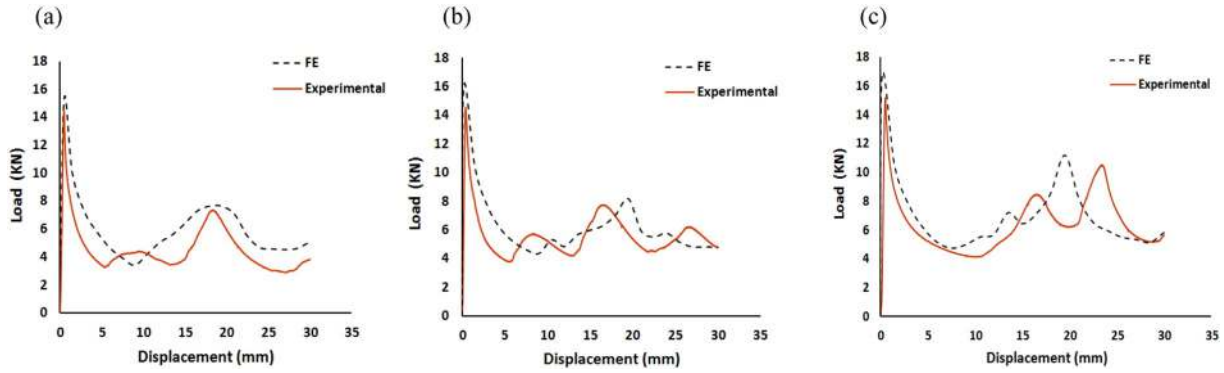

Fig. 12. Numerical and experimental load–displacement curves for (a) EST, (b) CFFST and (c) AFFST.

where σ_c and ε_{axial}^{Pl} are the compressive stress and axial plastic strain due to compression, respectively. The elastic behavior is modeled only as linear elastic as shown in Eq. (17).

$$\sigma = D^{el} : \varepsilon^{el} \tag{17}$$

where D^{el} represents the fourth-order elasticity tensor and σ and ε^{el} are the second-order stress and elastic strain tensors, respectively.

The true stress–strain curve data points and material properties obtained from Fig. 6(b) were utilized for calibrating the foam materials model.

5. Crush response and energy absorption performances

Fig. 11 shows the deformation modes of EST, CFFST and AFFST, experimentally and numerically. Since the main objective of the present research is to investigate the global behavior of auxetic foam-filled tubes under axial loading, the effect of localized buckling has then been ignored in the simulation. Nonetheless, the numerical and experimental results show a good agreement. Load–displacement curves of the samples achieved from experiments and FE simulations have been plotted and compared in Fig. 12. It is evident that a good correlation between the results has been achieved. As mentioned earlier, each experimental test includes 5 samples. The experimental results are almost identical with the standard deviations of 1.78, 1.94 and 1.97 for EST, CFFST and AFFST, respectively. Likewise, the standard errors for the EST, CFFST and AFFST are 0.8, 0.87 and 0.93, respectively. Thus, the average data were used for the crashworthiness assessment.

There are several indicators to evaluate the crashworthiness of axial crushing of a structure and to design a controllable crushing pattern for maximizing energy absorption and allowable peak forces during the collapse. In present study, peak force (P_{max}), energy absorption (EA), mean crush force (P_m), specific energy absorption (SEA) and crush force efficiency (CFE) are the parameters which are used in measuring crashworthiness [69]. The P_{max} demonstrates the force needed to initiate collapse and to commence the energy absorption process. Energy absorption (EA) is a criterion to specify the stable limit of a structure and allows a comparison among different designs. During axial crushing, the EA is calculated via Eq. (18).

$$EA(d) = \int_0^d F(\delta)d\delta \tag{18}$$

where d and δ are the crushing distance and displacement respectively and F denotes the crushing force. In particular, the area under the load displacement curve is equal to energy absorption capacity. The mean crush force (P_m), based on the EA can be determined using Eq. (19) [70].

$$P_m = \frac{EA}{\delta}. \tag{19}$$

In particular, P_m for a given deformation indicates capacity of energy absorption of a structure. The absorbed energy per unit mass of a structure namely SEA is formulated as follows.

$$SEA = \frac{EA}{m} \tag{20}$$

where m is the mass of the structure. It means that a greater SEA leads to a better capacity of energy absorption with respect to the mass of the structure. The CFE of a structure as the other key indicator is calculated as follows.

$$CFE = \frac{P_m}{P_{\max}} \times 100\%. \tag{21}$$

Table 2
Numerical and experimental results from axially compressed specimens.

Samples	Experimental					FE simulation				
	EA (J)	P_{max} (kN)	P_m (kN)	SEA (kJ/kg)	CFE (%)	EA (J)	P_{max} (kN)	P_m (kN)	SEA (kJ/kg)	CFE (%)
EST	136.2	14.1	4.5	10	29.8	157.2	15.2	5.2	11.6	32.8
CFFST	168.4	14.2	5.6	11.1	37.5	185.8	16.2	6.2	12.2	38.8
AFFST	192.5	15.8	6.4	11.8	38.5	206.8	16.9	6.9	12.7	39.3

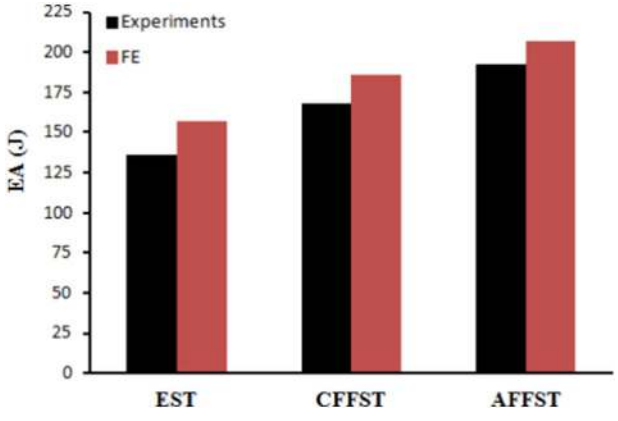

Fig. 13. Comparison between numerical and experimental values of EA of samples.

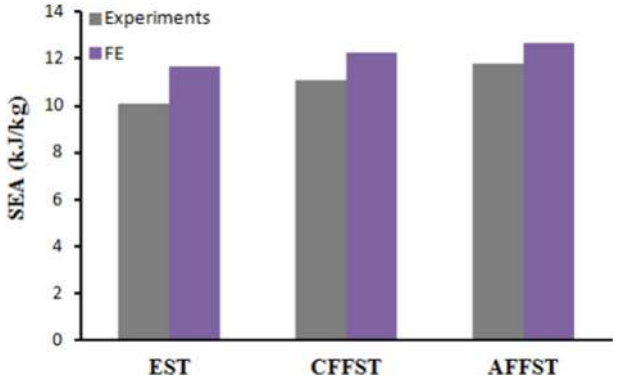

Fig. 14. Comparison between numerical and experimental values of *SEA* of samples.

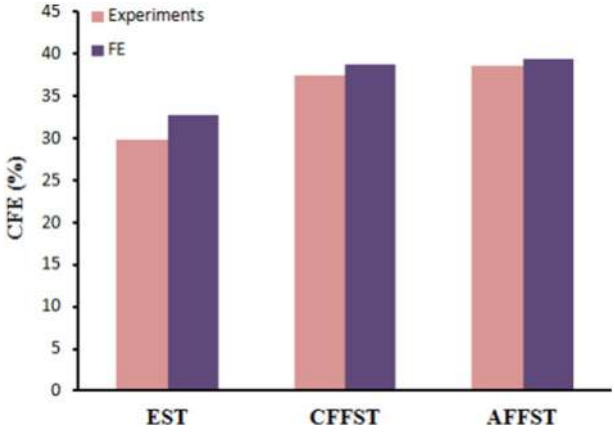

Fig. 16. Comparison between numerical and experimental values of CFE of samples.

The *CFE* determines the uniformity of load–displacement curve of the crushing process. It means higher *CFE* illustrates a more ideal energy absorption characteristic.

The value of all crashworthiness indictors used in this study is tabulated in Table 2. Also, for better comparison and understanding, the FE and experimental results of *EA*, *SEA*, P_m and *CFE* are shown in Figs. 13 to 16. By referring to Table 2 and Figs. 13 to 16, it is noteworthy that the FE results are always slightly higher than the experimental results. This common discrepancy between these two results is due to the perfect FE model employed without considering any probable defect in the tube and foam materials caused by manufacturing process. Moreover, in FE simulation, the contact surface between foam and tube has been modeled perfectly without any gap between the foam and tube.

From Fig. 12 and Table 2, the initial P_{max} of the AFFST is slightly higher than that of the EST and CFFST which is surprisingly undesirable in crashworthiness applications. However, this initial onset load effect may be compromised with a greater energy absorption capacity obtained. This may be due to the NPR of auxetic material which made the extra absorbent layers along the impact load transmission path. Considering the higher strength of tube than foams, the study of P_{max} may not singly enough and second peak load in load–displacement curves can assist to better evaluate the crashworthiness ability. From Fig. 12, the onset of second peak load in AFFST is almost two times and 30% greater than that of the EST and CFFST, respectively. It leads to the increase in P_m (Fig. 15 and Table 2) which leads to enhance the resistance ability of structure versus impact loading. Thus, the crashworthiness performance of structure becomes more impressive.

From Fig. 13, concerning the energy absorption capacity, it is obvious that the AFFST is advantageous over the other configurations in EST and CFFST. It can be attributed to the toughness of auxetic foam which is an important mechanical property since specifies the maximum *EA* of the foam per unit. Toughness can be calculated by integrating the area under stress–strain curve. As a result of converting into the auxetic, the foam toughness increases [37] and causes to enhance the area under load–displacement curve which improves the *EA* capacity. Hence, the *EA* of the AFFST is 14.3% higher than that of the CFFST and 41.3% than that of the EST.

In Fig. 14, it is noted that as a CFFST changes to an AFFST, its *SEA* increases at around 14%. It can also be highlighted that AFFST has 23% greater *SEA* than EST. It means that despite of increasing the weight of structure in AFFST, better capacity of energy absorption for this tube can be obtained. By using auxetic foam, the structure becomes heavier which is inevitable due to densification process during converting conventional foam into the auxetic foam. Although increasing density is the predominant effect of auxeticity phenomenon, the main influence of increasing energy absorption capacity is due to the changing of microstructure during the converting process from conventional into the auxetic. This micro-structural variations lead to obtain the NPR. Previous most cited studies [46,50,71] showed that in parallel of increasing in NPR, the indentation resistance and toughness are enhanced remarkably. The former causes to increase the initial peak loads and the latter leads to enhance energy absorption capacity. Furthermore, the energy absorption can be increased by using conventional foams with higher densities; this however is not always desirable as it results in a higher stiffness [58,72].

Fig. 15 shows that the P_m of AFFST is greater than that of CFFST, while the P_m of CFFST is greater than that of EST, i.e., using the auxetic foam as the filler. The more absorbed energy obtains for a given deformation.

Fig. 16 depicts the CFE of EST, CFFST and AFFST. It is evident that using auxetic foam has a relatively more noticeable influence on the crushing efficiency as the CFE of the AFFST is about 1.29 times higher than that of the EST and almost 3% greater than that of the CFFST. It means that the similarity of load–displacement curves, AFFST is the more efficient structure. It can arise from the NPR of auxetic foam, i.e. when it is subjected to compressive load, the force compresses the foam, and the foam compensates by spreading in the directions perpendicular to and away from the direction of the load. In fact, the material flows into (compresses towards) the vicinity of the load. This creates an area of denser material, which is more resistant to impact and becomes more efficient for the energy absorption.

The tested samples were cut in order to evaluate the deformation mode profiles after loaded, as shown in Fig. 17. It is evident that the type and number of folds in the EST are different than that of the CFFST and AFFST. The effect of localized bulking is explicitly visible in the edge of the EST sample. Although the effect of localized bulking in CFFST has decreased, the area between the folds has not been filled completely. Thus, using the conventional foam as the filler could not provide the progressive collapse during the loading process. In the AFFST, the area between folds has been remarkably filled even though

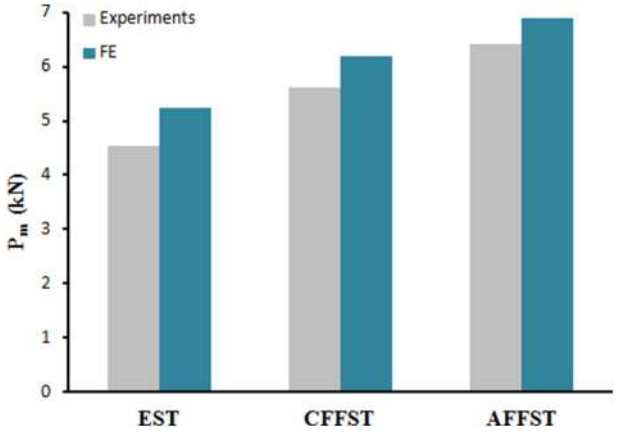

Fig. 15. Comparison between numerical and experimental values of mean crushing load of samples.

Fig. 17. Cutting sections of the tested samples; (a) EST, (b) CFFST, (c) AFFST.

no bonding has been used to connect the foam and tube. From a theoretical point of view, changing the conventional foam microstructure into the auxetic leads to obtain the NPR [56]. The fabrication of auxetic foam with a higher range of negative Poisson's ratio causes to achieve a microstructure with low Pores per Inches (PPI). In particular, a higher NPR determines the degree of re-entrancy of the cells and reduces the blank spaces in the auxetic microstructure [36,51]. Due to this low PPI, when the auxetic foam is compressed up to the densification region, it starts to expend laterally. This lateral expansion in conventional foams is far less obvious due to the higher PPI. Therefore, the possible reason of more desired foam filled area in the AFFST can be attributed to the re-entrant microstructure and its NPR. Thereby, the progressive collapse in the AFFST is more desirable comparing to the EST and CFFST. More importantly, the effect of localized bulking has been considerably decreased in the AFFST.

From the above-mentioned results of the AFFST, it reveals that achieving a well-filled collapsed tube wall may attribute to an increase in foam density (a decrease in PPI of auxetic structure) and NPR. In order to decouple the effects of density and Poisson's ratio, a series of additional experimental tests was conducted. The density and mechanical properties of the conventional and auxetic foams are approximately the same, yet different sign of Poisson's ratios used as the fillers in the tubes. Foams and their stress–strain curves are shown in Figs. 18 and 19, respectively. Specifications of foams are listed in Table 3.

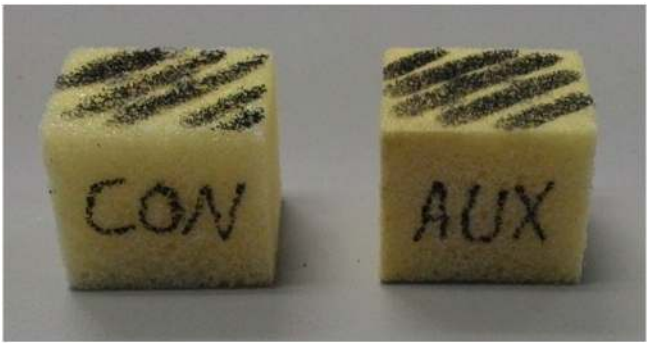

Fig. 18. Conventional and auxetic foam with approximately a similar density.

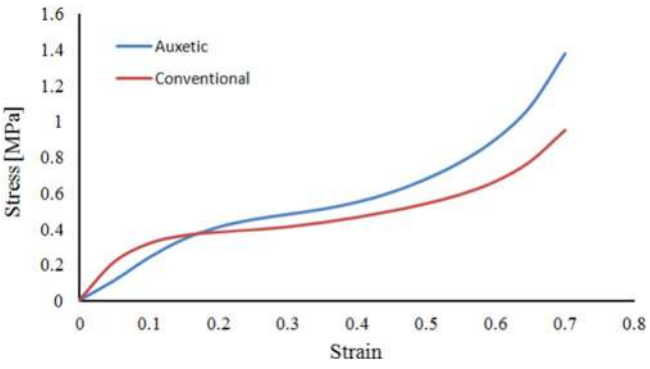

Fig. 19. Stress–strain curves of conventional and auxetic foams in additional experiments.

The finding is consistent with the earlier finding in which the AFFST is superior to the CFFST in energy absorption performance based on the energy absorption capacity and crush response. Tube configuration, deformation modes and load–displacement curves of the tested samples are depicted in Fig. 20.

From Fig. 20(c), it is obvious that the area between folds has been almost completely filled in the AFFST than that of CFFST even though the density of conventional and auxetic foams is approximately similar while they have different sign of Poisson's ratio. Nevertheless, the filled area in Fig. 17(c) is slightly greater than that in Fig. 20(c). This result reflects that the density of foam has also the substantial effect on the progressive collapse.

The experimental results of *EA* and *SEA* for these samples are depicted in Fig. 21. From Fig. 21(a), it is noteworthy that the AFFST is advantageous over the CFFST in terms of *EA* with 6.15% increment. Also, Fig. 21(b) indicates that as a CFFST changes to an AFFST, its *SEA* increases up to 7.11%. The present results confirm that howbeit NPR has a significant influence to obtain higher *EA* and *SEA*, the effect of an increase in the density of foam is also greatly considerable.

6. Conclusions

In this paper, the crashworthiness behavior of aluminum square tubes namely EST, CFFST and AFFST under quasi-static loading condition was experimentally and numerically studied. It shows a good agreement between the experiment outcomes and simulation results. A comparison of the results showed that the AFFST has greater *EA* in comparison with the other tubes. Overall, the AFFST exhibit 41.3% and 14.3% increment in *EA* than EST and CFFST, respectively. On the other hand, despite of the increase in the total weight of the structure of the AFFST, its SEA increases remarkably. Also an evaluation of the results indicated that the AFFST has greater mean crushing load and *CFE* in comparison with EST and CFFST. It shows that the AFFST offers more controllable crushing pattern with respect to maximizing energy absorption. In the case of deformation mode, the AFFST showed better progressive collapse in comparison with other tubes. Also the effect of localized bulking was far less observed in the AFFST than in the EST and CFFST. Above all, it is evident that a foam core with a negative Poisson's ratio has a significant influence in the progressive collapse of a thin-walled tube. However, results reflect that the density of foam

Table 3
Specification of foams.

Foam type	ρ (kg/m^3)	υ
Conventional	67.3	0.015
Auxetic	62.7	−0.19

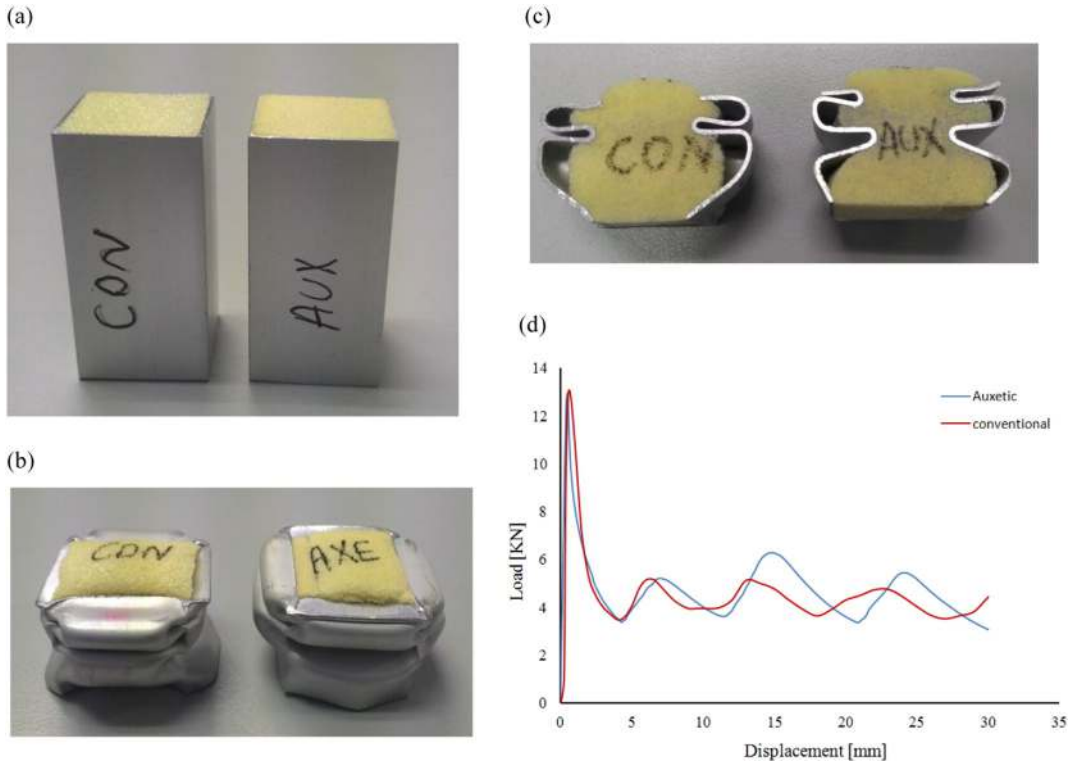

Fig. 20. Additional experimental tests; (a) tube configuration; (left) CFFST and (right) AFFST, (b) deformation modes (left) CFFST and (right) AFFST, (c) cutting sections of the tested samples; (left) CFFST and (right) AFFST, (d) load–displacement curves.

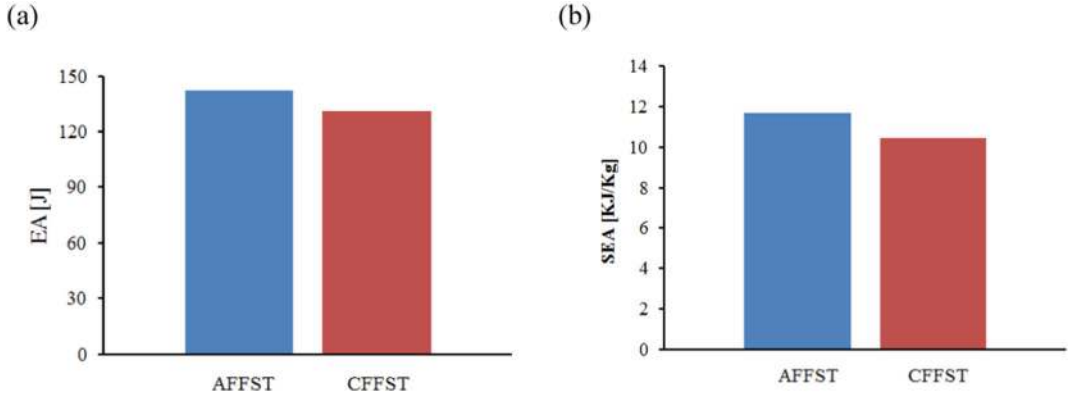

Fig. 21. Comparison between CFFST and AFFST for new samples (a) *EA* and (b) *SEA* in additional experiments.

has also the substantial effect on the progressive collapse. This study has focused on the effect of using auxetic foam as filler inside a square tube. Investigation of reliability of FE results in predicting the energy absorption of other geometrical shapes filled with auxetic foam can further be implemented in the future work. The present outcomes of this paper may be of high interest to those engineers who intend to utilize the auxetic foam in their crashworthy design.

References

[1] S. Liu, Z. Tong, Z. Tang, Y. Liu, Z. Zhang, Bionic design modification of non-convex multi-corner thin-walled columns for improving energy absorption through adding bulkheads, Thin-Walled Struct. 88 (2015) 70–81.
[2] R. Alipour, A.F. Nejad, S. Izman, The reliability of finite element analysis results of the low impact test in predicting the energy absorption performance of thin-walled structures, J. Mech. Sci. Technol. 29 (2015) 2035–2045.
[3] A. Alavi Nia, M. Parsapour, Comparative analysis of energy absorption capacity of simple and multi-cell thin-walled tubes with triangular, square, hexagonal and octagonal sections, Thin-Walled Struct. 74 (2014) 155–165.
[4] G. Zheng, S. Wu, G. Sun, G. Li, Q. Li, Crushing analysis of foam-filled single and bitubal polygonal thin-walled tubes, Int. J. Mech. Sci. 87 (2014) 226–240.
[5] K.R.F. Andrews, G.L. England, E. Ghani, Classification of the axial collapse of cylindrical tubes under quasi-static loading, Int. J. Mech. Sci. 25 (1983) 687–696.
[6] W. Abramowicz, N. Jones, Dynamic axial crushing of square tubes, Int. J. Impact Eng. 2 (1984) 179–208.
[7] W. Abramowicz, N. Jones, Dynamic progressive buckling of circular and square tubes, International Journal of Impact Engineering 4 (1986) 243–270.
[8] M. Langseth, O.S. Hopperstad, Static and dynamic axial crushing of square thin-walled aluminium extrusions, International Journal of Impact Engineering 18 (1996) 949–968.
[9] A. Alavi Nia, J. Haddad Hamedani, Comparative analysis of energy absorption and deformations of thin walled tubes with various section geometries, Thin-Walled Struct. 48 (2010) 946–954.
[10] W. Abramowicz, T. Wierzbicki, Axial crushing of foam-filled columns, Int. J. Mech. Sci. 30 (1988) 263–271.

[11] A.G. Hanssen, M. Langseth, O.S. Hopperstad, Static and dynamic crushing of circular aluminium extrusions with aluminium foam filler, International Journal of Impact Engineering 24 (2000) 475–507.
[12] S.R. Reid, T.Y. Reddy, Static and dynamic crushing of tapered sheet metal tubes of rectangular cross-section, Int. J. Mech. Sci. 28 (1986) 623–637.
[13] Z. Ahmad, D.P. Thambiratnam, Application of foam-filled conical tubes in enhancing the crashworthiness performance of vehicle protective structures, International Journal of Crashworthiness 14 (2009) 349–363.
[14] M. Seitzberger, F.G. Rammerstorfer, R. Gradinger, H.P. Degischer, M. Blaimschein, C. Walch, Experimental studies on the quasi-static axial crushing of steel columns filled with aluminium foam, Int. J. Solids Struct. 37 (2000) 4125–4147.
[15] N.K. Gupta, P. Ray, Collapse of thin-walled empty and filled square tubes under lateral loading between rigid plates, International Journal of Crashworthiness 3 (1998) 265–285.
[16] T. Børvik, O.S. Hopperstad, A. Reyes, M. Langseth, G. Solomos, T. Dyngeland, Empty and foam-filled circular aluminium tubes subjected to axial and oblique quasistatic loading, International Journal of Crashworthiness 8 (2003) 481–494.
[17] S.P. Santosa, T. Wierzbicki, A.G. Hanssen, M. Langseth, Experimental and numerical studies of foam-filled sections, International Journal of Impact Engineering 24 (2000) 509–534.
[18] L. Aktay, A.K. Toksoy, M. Güden, Quasi-static axial crushing of extruded polystyrene foam-filled thin-walled aluminum tubes: experimental and numerical analysis, Mater. Des. 27 (2006) 556–565.
[19] C.P. Gameiro, J. Cirne, Dynamic axial crushing of short to long circular aluminium tubes with agglomerate cork filler, Int. J. Mech. Sci. 49 (2007) 1029–1037.
[20] Z. Ahmad, D.P. Thambiratnam, Crushing response of foam-filled conical tubes under quasi-static axial loading, Mater. Des. 30 (2009) 2393–2403.
[21] Z. Ahmad, D.P. Thambiratnam, Dynamic computer simulation and energy absorption of foam-filled conical tubes under axial impact loading, Comput. Struct. 87 (2009) 186–197.
[22] Z. Ahmad, D.P. Thambiratnam, A.C.C. Tan, Dynamic energy absorption characteristics of foam-filled conical tubes under oblique impact loading, International Journal of Impact Engineering 37 (2010) 475–488.
[23] L. Mirfendereski, M. Salimi, S. Ziaei-Rad, Parametric study and numerical analysis of empty and foam-filled thin-walled tubes under static and dynamic loadings, Int. J. Mech. Sci. 50 (2008) 1042–1057.
[24] S. Santosa, T. Wierzbicki, Crash behavior of box columns filled with aluminum honeycomb or foam, Comput. Struct. 68 (1998) 343–367.
[25] I. Duarte, M. Vesenjak, L. Krstulović-Opara, Dynamic and quasi-static bending behaviour of thin-walled aluminium tubes filled with aluminium foam, Compos. Struct. 109 (2014) 48–56.
[26] I. Duarte, M. Vesenjak, L. Krstulović-Opara, I. Anžel, J.M.F. Ferreira, Manufacturing and bending behaviour of in situ foam-filled aluminium alloy tubes, Mater. Des. 66 (2015) 532–544 Part B.
[27] G. Sun, G. Li, S. Hou, S. Zhou, W. Li, Q. Li, Crashworthiness design for functionally graded foam-filled thin-walled structures, Mater. Sci. Eng. A 527 (2010) 1911–1919.
[28] H. Yin, G. Wen, X. Wu, Q. Qing, S. Hou, Crashworthiness design of functionally graded foam-filled multi-cell thin-walled structures, Thin-Walled Struct. 85 (2014) 142–155.
[29] Y. Prawoto, Seeing auxetic materials from the mechanics point of view: a structural review on the negative Poisson's ratio, Comput. Mater. Sci. 58 (2012) 140–153.
[30] Z.-X. Lu, Q. Liu, Z.-Y. Yang, Predictions of Young's modulus and negative Poisson's ratio of auxetic foams, Phys. Status Solidi B 248 (2011) 167–174.
[31] K.E. Evans, M.A. Nkansah, I.J. Hutchinson, S.C. Rogers, Molecular network design [12], Nature 353 (1991) 124.
[32] A.E.H. Love, A Treatise on the Mathematical Theory of Elasticity, Dover Publications, New York, 1944.
[33] M. Bianchi, F. Scarpa, C.W. Smith, Shape memory behaviour in auxetic foams: mechanical properties, Acta Mater. 58 (2010) 858–865.
[34] M. Shokri Rad, Y. Prawoto, Z. Ahmad, Analytical solution and finite element approach to the 3D re-entrant structures of auxetic materials, Mech. Mater. 74 (2014) 76–87.
[35] C.W. Smith, J.N. Grima, K.E. Evans, A novel mechanism for generating auxetic behaviour in reticulated foams: missing rib foam model, Acta Mater. 48 (2000) 4349–4356.
[36] M. Bianchi, F. Scarpa, M. Banse, C.W. Smith, Novel generation of auxetic open cell foams for curved and arbitrary shapes, Acta Mater. 59 (2011) 686–691.
[37] A. Bezazi, F. Scarpa, Mechanical behaviour of conventional and negative Poisson's ratio thermoplastic polyurethane foams under compressive cyclic loading, Int. J. Fatigue 29 (2007) 922–930.
[38] P. Subramani, S. Rana, D.V. Oliveira, R. Fangueiro, J. Xavier, Development of novel auxetic structures based on braided composites, Mater. Des. 61 (2014) 286–295.
[39] M. Uzum, Mechanical properties of auxetic and conventional polypropylene random short fiber reinforced composites, FIBRES TEXT East Eur, 20 2012, pp. 70–74.
[40] J.N. Grima, R. Caruana-Gauci, D. Attard, R. Gatt, Three-Dimensional Cellular Structures with Negative Poisson's Ratio and Negative Compressibility Properties, 2012.
[41] M. Bianchi, F. Scarpa, C. Smith, Stiffness and energy dissipation in polyurethane auxetic foams, J. Mater. Sci. 43 (2008) 5851–5860.
[42] M. Sanami, N. Ravirala, K. Alderson, A. Alderson, Auxetic materials for sports applications, Prod. Eng. 72 (2014) 453–458.
[43] E. Cherubina, N. Petrone, Development of a new method for the engineering predesign of sport helmets, Prod. Eng. 72 (2014) 483–488.
[44] J. Smardzewski, R. Kłos, B. Fabisiak, Design of small auxetic springs for furniture, Mater. Des. 51 (2013) 723–728.
[45] Y. Liu, H. Hu, A review on auxetic structures and polymeric materials, Sci. Res. Essays 5 (2010) 1052–1063.
[46] R. Critchley, I. Corni, J.A. Wharton, F.C. Walsh, R.J.K. Wood, K.R. Stokes, A review of the manufacture, mechanical properties and potential applications of auxetic foams, Phys. Status Solidi B (2013) 1–20.
[47] M.N. Ali, I.U. Rehman, Auxetic polyurethane stents and stent-grafts for the palliative treatment of squamous cell carcinomas of the proximal and mid oesophagus: a novel fabrication route, J. Manuf. Syst.
[48] K.E. Evans, A. Alderson, Auxetic materials: functional materials and structures from lateral thinking! Adv. Mater. 12 (2000) 617–628.
[49] A.G. Kolpakov, Determination of the average characteristics of elastic frameworks, J. Appl. Math. Mech. 49 (1985) 739–745.
[50] R. Lakes, Foam structures with a negative Poisson's ratio, Science 235 (1987) 1038–1040.
[51] E.A. Friis, R.S. Lakes, J.B. Park, Negative Poisson's ratio polymeric and metallic foams, J. Mater. Sci. 23 (1988) 4406–4414.
[52] J.N. Grima, D. Attard, R. Gatt, R.N. Cassar, A novel process for the manufacture of auxetic foams and for their re-conversion to conventional form, Adv. Eng. Mater. 11 (2009) 533–535.
[53] M. Bianchi, S. Frontoni, F. Scarpa, C.W. Smith, Density change during the manufacturing process of PU–PE open cell auxetic foams, Phys. Status Solidi B 248 (2011) 30–38.
[54] R. Lakes, No contractile obligations, Nature 358 (1992) 713–714.
[55] J.B. Choi, R. Lakes, Design of a fastener based on negative Poisson's ratio foam, Cell. Polym. 10 (1991) 205–212.
[56] N. Chan, K.E. Evans, Fabrication methods for auxetic foams, J. Mater. Sci. 32 (1997) 5945–5953.
[57] R. Lakes, Deformation mechanisms in negative Poisson's ratio materials: structural aspects, J. Mater. Sci. 26 (1991) 2287–2292.
[58] J.B. Choi, R.S. Lakes, Non-linear properties of polymer cellular materials with a negative Poisson's ratio, J. Mater. Sci. 27 (1992) 4678–4684.
[59] N. Chan, K.E. Evans, Microscopic examination of the microstructure and deformation of conventional and auxetic foams, J. Mater. Sci. 32 (1997) 5725–5736.
[60] L. Gibson, M. Ashby, G. Schajer, C. Robertson, The mechanics of two-dimensional cellular materials, Proceedings of the Royal Society of London A: Mathematical, Physical and Engineering Sciences, The Royal Society 1982, pp. 25–42.
[61] I.G. Masters, K.E. Evans, Models for the elastic deformation of honeycombs, Compos. Struct. 35 (1996) 403–422.
[62] J.K. Fink, 2 - Polyurethanes, in: J.K. Fink (Ed.), Reactive Polymers Fundamentals and Applications, William Andrew Publishing, Norwich, NY 2005, pp. 69–138.
[63] R.D. Widdle Jr., A.K. Bajaj, P. Davies, Measurement of the Poisson's ratio of flexible polyurethane foam and its influence on a uniaxial compression model, Int. J. Eng. Sci. 46 (2008) 31–49.
[64] L.L. Wang, D.S. Li, X.Q. Li, L. Wang, W.J. Yang, Coefficient of friction for aluminum alloy sheet in contact with polyurethane rubber, Appl. Mech. Mater. 26 (2010) 320–325.
[65] W. Tanwongwan, J. Carmai, Finite element modelling of titanium foam behaviour for dental application, Proceedings of the World Congress on Engineering, 2011.
[66] G. da Costa Machado, M.K. Alves, H.A. Al-Qureshi, R. Rossi, Constitutive Modeling of the Large Strain Behavior of Crushable Foams Using the Element-Free Galerkin Method.
[67] T. Hibbitt, E. Karlsson, T. Sorensen, ABAQUS, Theory Manual, Hibbitt, Karlsson and Sorensen, 1997.
[68] A.P. Suvorov, G.J. Dvorak, Enhancement of low velocity impact damage resistance of sandwich plates, Int. J. Solids Struct. 42 (2005) 2323–2344.
[69] F. Xu, G. Sun, G. Li, Q. Li, Experimental study on crashworthiness of tailor-welded blank (TWB) thin-walled high-strength steel (HSS) tubular structures, Thin-Walled Struct. 74 (2014) 12–27.
[70] B.W. Williams, D.A. Oliveira, C.H.M. Simha, M.J. Worswick, R. Mayer, Crashworthiness of straight section hydroformed aluminium tubes, International Journal of Impact Engineering 34 (2007) 1451–1464.
[71] S. Timoshenko, J. Goodier, H.N. Abramson, Theory of elasticity, J. Appl. Mech. 37 (1970) 888.
[72] F. Scarpa, J. Yates, L. Ciffo, S. Patsias, Dynamic crushing of auxetic open-cell polyurethane foam, Proc. Inst. Mech. Eng. C J. Mech. Eng. Sci. 216 (2002) 1153–1156.